

Numerical Model of Tube Freeform Bending by Three-Roll-Push-Bending

H. Hagenah¹, D. Vipavc¹, R. Plettke¹, M. Merklein¹

¹ Chair of Manufacturing Technology, Friedrich-Alexander University of Erlangen-Nuremberg

Abstract

Three-roll-push-bending is an innovative tube bending technology characterized by high flexibility. Only one toolkit per tube diameter is necessary to achieve any desired part geometry. The settings of the process parameters vary depending on the tube's material and geometry properties. The process design is performed by a set of characteristic lines describing the dependence of the bending radius on the setting roll position. Up to now the definition of the characteristic lines was based on empirical procedures requiring substantial numbers of experiments leading to a notable downtime of the machine. A few numerical models, based on the method of finite elements, were developed in order to reduce the machine's downtime. The latest developed FE-model is presented in this paper. In order to overcome some imperfections of the earlier numerical models of the process and based on the experience gathered with them, special emphasis was put on the modeling of the machine's deflection. The model was optimized by adjusting the rolls deflection characteristics to minimize the difference between computation and experiment. The paper will close with a comparison of the experimental and computational results of the previous and the adjusted model.

Keywords: Three-roll-push-bending, tube bending, finite element method, optimization

1. Introduction

Bent metal tubes find widespread application in many industrial sectors. A fabricated tube, either welded or extruded in straight tube sections, usually has to undergo post-fabrication treatments. In order to be formed into a usable product, it is mainly manufactured by special handcraft tools or by computer-controlled machines, where the part geometry can be obtained by means of either tool-dependent or kinematical processes [1].

The tool-dependent tube bending technologies, like for example the rotary draw bending process, have reached a high degree of reliability and robustness but suffer from a lack of flexibility, since each tool only be used to bent one constant radius for one outer diameter of the tube [2].

The three-roll-push-bending process is labeled as flexible since the geometry of the tube is defined by the position of the tool rolls and not by their diameter. Only one toolset per tube's outer diameter is needed to bend arbitrary radii within the process limits. In fact, since the tube is only punctual clamped between rolls and pushed through, the largest part of the tube is unconstrained during the process, thus no geometry supporting tool is needed.

1.1. The three-roll-push-bending process

A set of tools for the three-roll-push-bending process discussed in this research is shown in figure 1. The process, based on two holding rolls, one bending roll and one setting roll, is driven by axes which are numerical controlled. Among these the C-axis designates the feed of the tube. The setting roll is moved in the bending plane by either rotating around the centre of the bending roll (Y-axis) or translating in radial direction (P-axis). Although three rolls are sufficient to perform the bending operation, a rear holding roll is used to stabilize the tube during the bending operation.

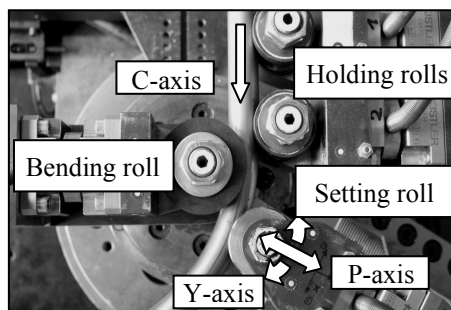


Figure 1: Tools and axis of the three-roll-push-bending machine

The three-roll-push-bending process can be described by three steps as displayed in figure 2. The set-up stage includes the clamping of the tube and the closing of the tool. After this the starting step follows where the setting

roll is moved to the end position with a simultaneous feeding of the tube, which is performed by the C-axis. When the desired position of the setting roll is reached, a constant radius R is bent by constant feeding of the tube.

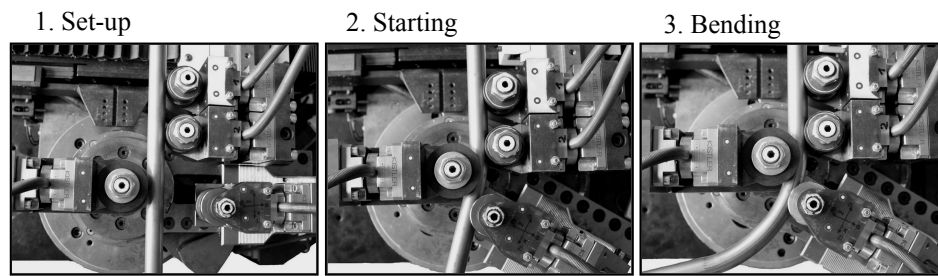


Figure 2: Three main steps of the tree-roll-push-bending process

An arc is formed depending on the position of the setting roll defined by P- and Y-axis and the feeding rate of the C-Axis. As the setting roll can be moved while the tube is being pushed forward and since the machine has an additional A-axis allowing for rotation of the tube around the C-axis during the bending process, arbitrary 3D geometries can be bent. However, this paper will be limited to bending constant radii in the plane.

1.2. Influence factors of the three-roll-push-bending process

In the tree-roll-push-bending process the bending radius is the result of the kinematic-dynamic conditions that occur during the bending process. The bending radius is affected by many influences that can either be attributed to the tube or to the machine. Some of them are known before the process and can be controlled (factors) while others are beyond control (cofactors). An overview is given in table 1.

Table 1: Influences on the bending radius

	Factors	Cofactors	Result
Machine	Process parameters - P-axis - Y-axis - C-axis	- Machine deflection - Friction conditions - ...	Bending radius - $R[mm]$
Tube	Geometry parameters - Inner diameter d - Outer diameter D - Tube's length l Material parameters - Poisson's ratio ν - Young's modulus E - Hardening curve $\sigma(\epsilon)$	- Batch variations of material - Springback - ...	

The process parameters have the biggest effect on the bending radius and are controlled by the machine. Geometry and material parameters are defined as tube properties by elastic and plastic properties and can vary due to batch variations of the material. The effect of batch variations of material has not yet been researched. Beside these also cofactors like the machine's deflection affect the resulting radius. The feed of the C-axis gives the tube an energy which is mainly used for the elastic plastic bending work. However, this energy is also partly dissipated through the deflection of the machine. Beside these cofactors also friction conditions and springback are important. Friction occurs between the tube and the rolls, it has been found small in experiments. Springback occurs during the three-roll-push-bending process, but has not been quantified or modeled so far.

1.3. The process design

The bending plane, as shown in figure 3, can be introduced as a polar coordinate system with a dislocated center of rotation in the bending roll. Each position of the setting roll in the bending plane represents one combination of the values for the P- and Y-axis with corresponding bending radius R .

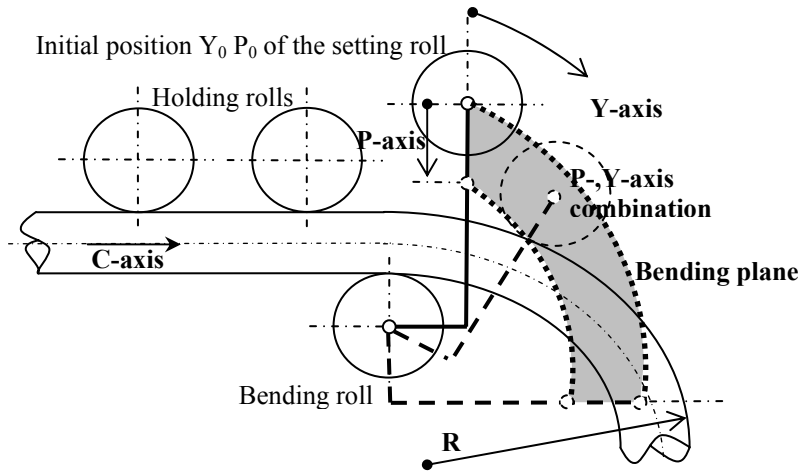


Figure 3: Schematic representation of the bending plane

In order to determine the P/Y-combination to be used to manufacture a desired radius, the bending plane, which consists of an infinite number of P- and Y-axis combinations, is approximated by a set of characteristic lines (figure 4). These are then used to control the bending machine Wafios BMZ 61, which represents in this case the three-roll-push-bending process. Each characteristic line of the set is interpolated on the basis of experimentally determined bending radii at a number of characteristic points (1):

$$R = f(P, Y) \quad (1)$$

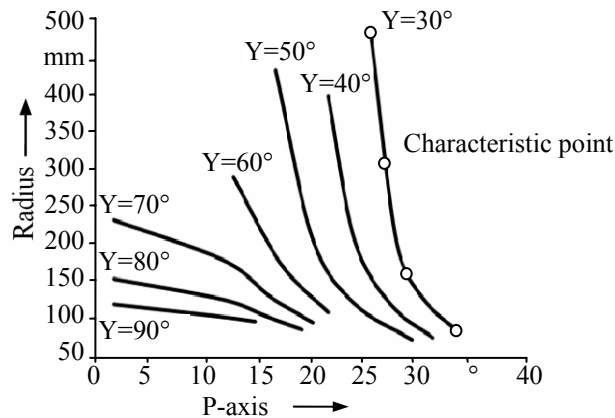


Figure 4: Set of characteristic lines for several parameter settings of the Y-axis

The set of characteristic lines is valid for one specific tube material and specific tube geometry given by the outer diameter and the wall thickness. If only one of these parameters is changed the whole procedure of characteristic line determination has to be repeated. Experience has shown that the determination of the characteristic lines leads to inconvenient production downtime. A different approach to determine the relation between bending radius and setting roll position without the need of extensive experimental work has been presented in [3].

1.4. Previous work

By now a few numerical models based on the method of finite elements FEM has been implemented. The previous FE-model modeled in PAM-STAMP 2G (ESI Group) [4], was constrained only by the controllable factors, which are explained in table 1. The resulting shape of the part for a given material and tube geometry was only depending on the position of the setting roll. This position was defined by kinematical equations which translate the original P- and Y-axis from the polar coordinate system into a Cartesian coordinate system. The machine's deflection was not considered in the previous model. As measurements of the machine's deflection showed a significant influence of this cofactor on the resulting radius it could be understood, that computational results with earlier models did not meet experimental results within an acceptable 5% deviation. In order to overcome this, the improved FE-model was developed.

2. The development of the improved FE-model

Considering the three-roll-push-bending process characteristics the improved FE-model was developed in the FE-software ABAQUS 6.8. The model was set up by importing and meshing the tool's geometry from available CAD-models of the tools. In order to adapt the numerical model to real process behavior, the roll positions were defined by digitizing the closed tool positions using an optical measurement system.

Experimental investigations were conducted for tubes made of carbon steel St 37 with an outer diameter of 20mm and a wall thickness of 1mm [5]. The same tube was modelled in CAD-software and used for the numerical experiments. The tube discretization was performed by four node shell elements (S4R) with five integration points and an hourglass control [6]. The size of the elements was 1.4mm x 1.4mm. In order to model tube's with a length of 500mm a step time of 0.35 s was set and solved using Abaqus/Explicit. An isotropic elastic material model defining the Young's Modulus as 210 000N/mm² and the Poisson number to be 0.3 was used. Further input data for the description of the plastic isotropic behaviour of the material, like hardening curve and anisotropy values, were determined by appropriate testing procedures. The tensile test was employed to determine the hardening curve [7]. The interaction properties between tools and tube were adapted in the same way as in the previous FE-model.

As mentioned before special emphasis was put on the modelling of the machine's deflection.

2.1. Simulation of the machine's deflection

The machine's deflection summarizes the effect resulting from each single roll deflecting when a force is applied. The three-roll-push-bending process can be observed as an energy balanced model:

$$E_I + E_V + E_{FR} + E_K - E_W = E_{total} \quad (2)$$

where E_I is the internal energy introducing elastic and plastic strain energy to the tube. E_V is the energy causing the machine's deflection. E_{FR} is the energy absorbed by the frictional dissipation between rolls and tube and was neglected as it was found very small in experiments. E_K is the kinetic energy of the tube. Since the speed of the tube is small, the kinetic energy was neglected as well. E_W is the work introduced by external forces, namely the feed of the C-axis, and E_{total} is the total energy of the system.

The dissipation of the energy E_v results in the machine's deflection. To simulate this effect, the FE-model was considered as a system under the influence of forced vibration caused by time depending external forces. Generally, vibration is the periodic motion of a body or system of connected bodies displaced from a position of equilibrium [8]. The system was described by the most general case of single degree of freedom forced vibrating motion. The analysis of this particular type of vibration is of practical value when applied to a system having a significant damping characteristic. Thus, it is presumed, that the system can be described using the viscous damped forced vibration case as shown in figure 5.

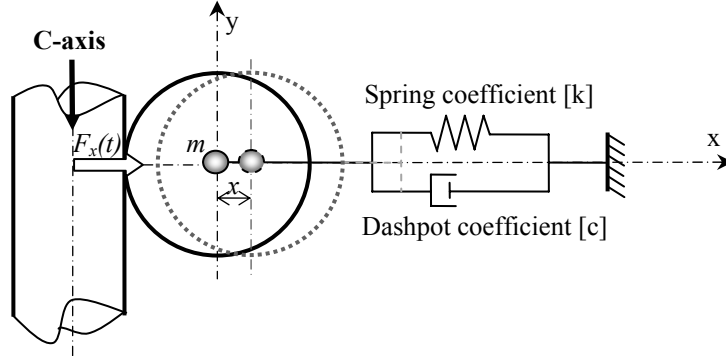


Figure 5: The vibration motion of a roll under viscous damping

The effect of damping is provided by the dashpot connected to the roll with the dashpot coefficient c . The spring represents the elastic deformation of the system and is characterized by the coefficient k . When the external force $F_x(t)$ is applied, the roll is displaced for a distance x . Both the spring force and the damping force oppose the motion of the roll, so that applying the equation of motion:

$$F_x(t) = m \cdot a_x \quad (2)$$

The derivatives of components in x direction are:

$$a_x = \dot{v}_x = \ddot{x} \quad (3)$$

The differential equation which describes the vibration case is:

$$m\ddot{x} + c\dot{x} + kx = F_x(t) \quad (4)$$

The differential equation represents a dashpot, which damps the vibrations caused by the time depending forces. The left side of equation frames the mass of the roll m which is accelerated and in the same time damped by a dashpot and spring, which represents the elastic deformation of the machine. The searched parameter is therefore the displacement of the roll x . In order to make the differential equation (4) solvable, the spring and dashpot coefficients have to be known. The spring coefficients k for all rolls were determined experimentally as described in section 2.2 while the dashpot coefficients c were determined manually and vary between 6 and 7 for the different rolls.

Both holding rolls and the bending roll were adapted to the vibration theory as shown figure 6. ABAQUS 6.8 offers a library, where connector section settings are predefined [9]. Connector section settings can be applied in order to define a connector element which connects two or more elements in one wired assembly with its own kinematical-dynamic features. In a more practical view, each roll was modeled as a connection between one fixed point in the global coordinate system and the one point representing the mass centre m of the roll. After the connections were defined, the connector section settings of each element had to be defined, i. e. the characteristics of the springs and dashpots.

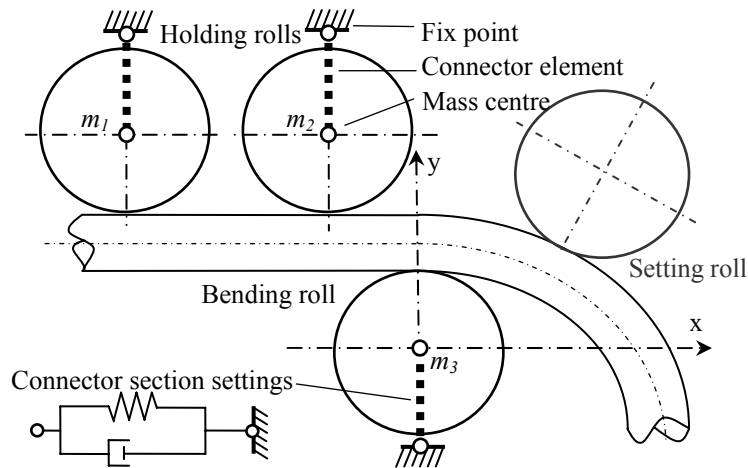


Figure 6: Definition of the connector section settings

The setting roll of the three-roll-push-bending-process is driven by the P- and Y-axis. In order to simulate its deflection, the guiding mechanism was modeled as displayed in figure 7.

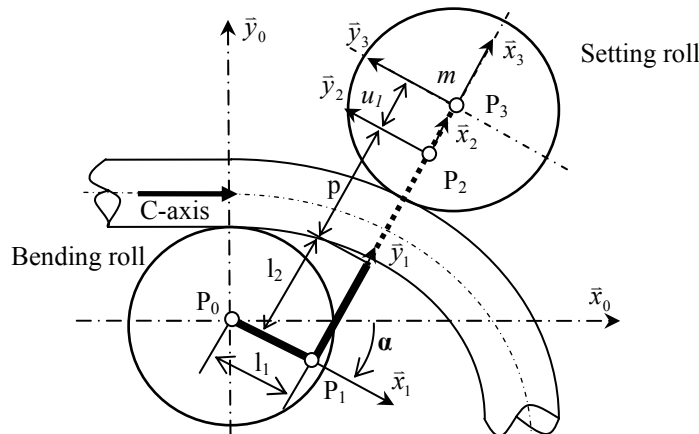


Figure 7: The guiding mechanism of the setting roll

The guiding mechanism has the shape of an L and is build by three elements. The first element, which is fixed at the first point placed in the center P_0 of the global coordinate system $\{\bar{x}_0, \bar{y}_0\}$ and extends for the length l_1 ending in point P_1 , can be rotated. This rotation in the global coordinate system simulates the Y-axis as variable α . Point P_2 is defined starting at P_1 and using the local coordinate system $\{\bar{x}_1, \bar{y}_1\}$. The element, which connects P_1 with P_2 , is the guiding of the P-axis. The setting of the P-axis is modeled as variable p . The element is split in two parts, where

l_2 is fixed and p is variable in length. The connection angle between the first and the second element is 90° . The final element of this model is a variable representing the deflection of the setting roll. The element which extends under the influence of the force for a defined length u_1 , is connected to P_2 , defined using the local coordinate system $\{\bar{x}_2, \bar{y}_2\}$ and P_3 in the local coordinate system $\{\bar{x}_3, \bar{y}_3\}$. The centre of the setting roll is P_3 . The roll's mass m is concentrated in this point. P_3 can thus be defined as a forward kinematical position using the homogenous transformation matrix T_n (5):

$$P_3 = \begin{pmatrix} x_3 \\ y_3 \\ 1 \end{pmatrix} = T_n \begin{pmatrix} 0 \\ 0 \\ 1 \end{pmatrix} \quad (5)$$

The T_n are homogenous transformation matrices defined for each of the four local coordinate systems as (6), where T_1 is the rotation and T_2, T_3 and T_4 represent the different translations:

$$\begin{pmatrix} x_3 \\ y_3 \\ 1 \end{pmatrix} = T_1 T_2 T_3 T_4 \begin{pmatrix} 0 \\ 0 \\ 1 \end{pmatrix} \quad (6)$$

Using the describing parameters introduced earlier, α, l_1, l_2, p and u_1 , the system of matrices is given as (7):

$$\begin{pmatrix} x_3 \\ y_3 \\ 1 \end{pmatrix} = \begin{pmatrix} \cos \alpha & \sin \alpha & 0 \\ -\sin \alpha & \cos \alpha & 0 \\ 0 & 0 & 1 \end{pmatrix} \begin{pmatrix} 0 & -1 & l_1 \\ 1 & 0 & 0 \\ 0 & 0 & 1 \end{pmatrix} \begin{pmatrix} 1 & 0 & l_2 + p \\ 0 & 1 & 0 \\ 0 & 0 & 1 \end{pmatrix} \begin{pmatrix} 1 & 0 & u_1 \\ 0 & 1 & 0 \\ 0 & 0 & 1 \end{pmatrix} \begin{pmatrix} 0 \\ 0 \\ 1 \end{pmatrix} \quad (7)$$

This can be summarized to a matrix describing the mechanism's kinematic (8):

$$\begin{pmatrix} x_3 \\ y_3 \\ 1 \end{pmatrix} = \begin{pmatrix} l_1 \cos \alpha + (l_2 + p + u_1) \sin \alpha \\ -l_1 \sin \alpha + (l_2 + p + u_1) \cos \alpha \\ 1 \end{pmatrix} \quad (8)$$

2.2. Experimental measurement of the machine's deflection

Adaptation of the FE-model to real conditions demanded experimental measurements of the machine's deflection. The measurements were needed to acquire the data for the definition of the spring elements. To do so, each roll of the three-roll-push-bending process has been equipped with sensors as shown figure 8.

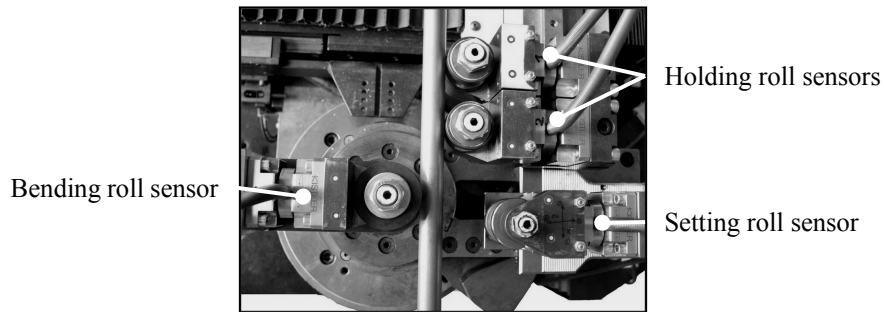


Figure 8: Rolls were equipped with a quartz 3-component force sensor

Quartz 3-component force sensors were used to measure the force acting in every direction of the rolls. Each roll was separately charged with a force F . The force was incrementally increased until the sensor's overload maximum was reached. For each increment the deflection of the roll was evaluated and described in a diagram called spring's characteristic function (SCF) $F(u)$ which replaces the spring coefficient k in equation (4).

On the left Figure 9 shows how the force which was produced by the holding rolls and transferred by a rod through the bending roll onto the setting roll. Measurement of the force F was done by the setting roll sensor and deflection u was noted by the measurement watch. Each measurement was repeated three times and the average values were used for the description of the spring elements. The right of figure 9 shows the results for the setting roll $F(u_1)$.

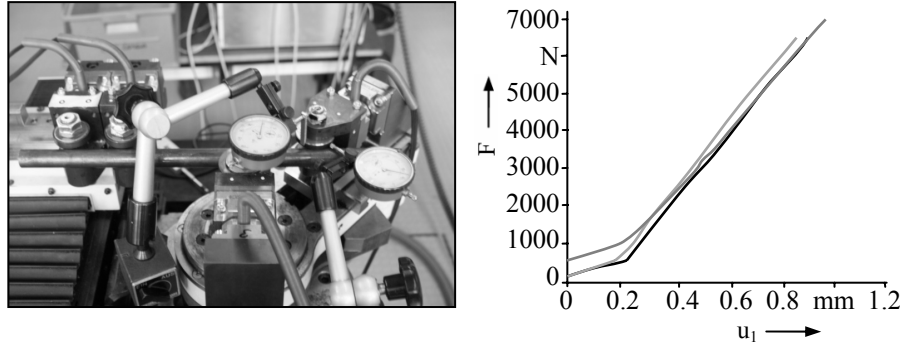


Figure 9: Measurement setup and resulting SCF $F(u_1)$ for the setting roll

The same procedure was then repeated in order to measure the bending roll and holding rolls deflections. The measured deflections are shown in figure 10. Since both holding rolls rest in the same holder they are modeled using the same SCF.

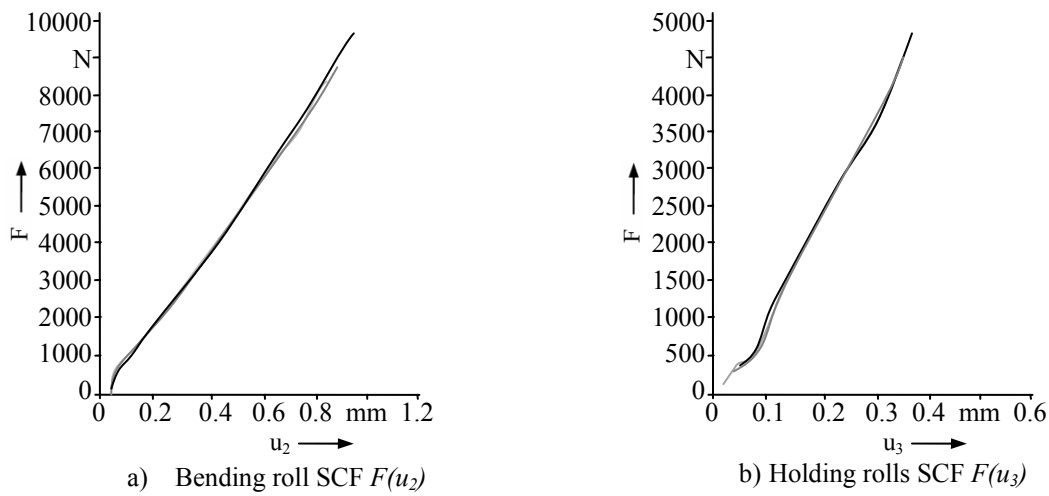


Figure 10: SCF for bending $F(u_2)$ and holding rolls $F(u_3)$

2.3. Validation of the FE-model

In order to validate the new FE-model, experimentally determined bending radii for the characteristic line with a constant value of $Y=35^\circ$ for one of the parameters were compared with the bending radii calculated by the FE-model. The results are shown in table 2.

Table 2: Deviations between experimental and computational bending radii

Y-axis [°]	P-axis [°]	Experimental R_{exp} [mm]	Simulative R_{sim} [mm]	Deviation R_{exp} and R_{sim} [%]	Deviation R_{exp} and R_{sim} [mm]
35	34	75.54	78.51	-3.92	-2.97
	30	123.36	118.83	3.67	4.53
	27	206.39	193.24	6.37	13.15
	24.5	443.34	410.97	7.43	32.37

The results show, that the precision of the FE-model varies depending on the bending radius. The smaller the radius the closer is the simulated bending radius to the experimentally determined one. Smaller bending radii result in bigger moments acting on the rolls. This means that the FE-model computes the deflections of the rolls quite precise, when the bending moments are relatively big. However, when larger radii are desired and consequently the moments are smaller, the simulated radii are outside of acceptable window of 5% deviation. The larger deviations might be explained as a result of the dynamic conditions occurring during the bending process. Those would result in different SCFs. As force and deflection during the dynamic process have not been measured, the adjustment of the SCF was seen as an optimization problem.

3. Optimization

Deflection of the FE-model is described with a spring and a dashpot, where the dashpot remains constant and the SCFs had to be adjusted. The goal of the optimization was the refinement of the SCFs in a way to make computational results meet the experimental data. To do so, the springs of the FE-model had to be adjusted to minimize the difference between computation and experiments, where the quality criterion used was the deviation of the simulated radius of the bent tube on the extrados from the experimentally determined radius. The objective function is given as follows (9):

$$f = \frac{1}{n} \sum_{i=0}^n \left| 1 - \frac{R_{\text{sim } i}}{R_{\text{exp } i}} \right| \quad (9)$$

where n represents the number of P- and Y-axis combinations, resulting in different bending radii. The experimental bending radii were taken from a previous study [5]. The study consists of 54 characteristic points, leading to experimental bending radii R_{exp} . To reduce the amount of simulations needed, these 54 characteristic points were reduced to 6 characteristic points which cover a wide spectrum of the load cases applied on the rolls. Table 3 shows the 6 characteristic points used in the optimization.

Table 3: Characteristic points

n	Y-axis [°]	P-axis [°]	Experimental R_{exp} [mm]
1	30	35	81.74
2	30	31.5	128.33
3	30	29	201.56
4	50	30.5	71.45
5	50	25	120.14
6	50	21	207.61

3.1. Optimization parameters (OP)

Figure 11 shows the FE-model consisting of four spring elements as described before in more detail. Each spring has its SCF $F(u_i)$ conducted by measurements.

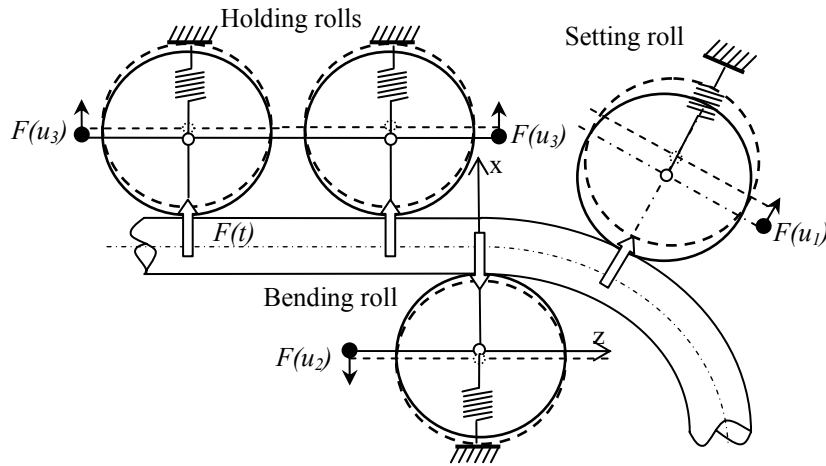


Figure 11: Modeling deflection with springs

In order to define an optimization problem, the generic SCFs shown in figures 9 and 10 had to be revised. Some simplifications were done. It was assumed that the holding rolls always respond in an equal linear way and can be observed as one system with one SCF $F(u_3)$. This linear function can be characterized by a single point K . Also the setting and bending roll springs show similar behavior under the load and can be modeled in the same way. Their SCFs were parameterized by two characteristic points M and L exhibiting a relatively simple two partial linear function. Thus the generic SCFs for all four springs were resembled as shown on the figure 12.

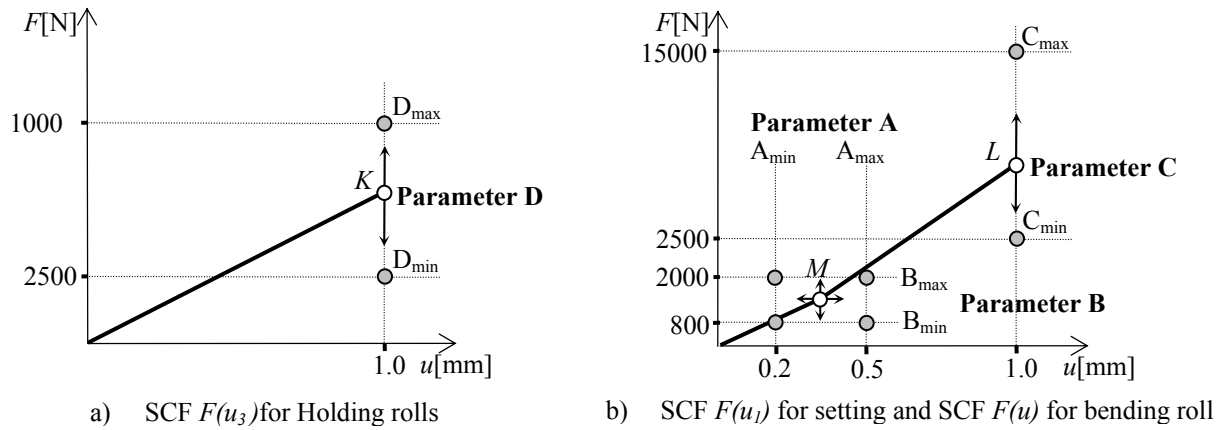


Figure 12: The diagram represents the parameterized SCFs of the rolls

Using this representation the optimization of the SCFs can be done by moving the K , L and M . The function $F(u_3)$ could be in this case be optimized by moving the point K between two constraining values (D_{min} , D_{max}). The SCFs $F(u_1)$ and $F(u_2)$ have two optimization points. Point M was defined to be moved between four constraining limits (A_{min} , B_{min} , A_{max} , B_{max}) in order to search for an optimum. Point L was varied between two constraining positions (C_{min} , C_{max}) and the optimum position was searched between these. In this way, seven optimization parameters were defined as shown in table 4.

Table 4: Optimization parameters

Roll	SCF	Optimization Parameters	Constrain
Setting roll	$F(u_1)$	$A_1 B_1 C_1$	$A_{min1} B_{min1} C_{min1} A_{max1} B_{max1} C_{max1}$
Bending roll	$F(u_2)$	$A_2 B_2 C_2$	$A_{min2} B_{min2} C_{min2} A_{max2} B_{max2} C_{max2}$
Holding rolls	$F(u_3)$	D	$D_{min} D_{max}$

3.3. Solution procedure

In order to find the best definition of the SCFs a full factorial test plan has been carried out using two levels for each optimization parameter and introducing one central point. The number of needed simulations is given in (13).

$$(A_1 \cdot B_1 \cdot C_1) \cdot (A_2 \cdot B_2 \cdot C_2) \cdot C_3 \cdot n + 1 = (2 \cdot 2 \cdot 2) \cdot (2 \cdot 2 \cdot 2) \cdot 2 \cdot 6 + 1 = 769 \quad (13)$$

Each of the 769 computations took approximately 45 minutes on a four kernel average PC. The results were entered in the objective function (9). As a result, 769 deviations between the simulated and the experimentally derived bending radii were determined. This result was represented in the shape of the response surface, which was approximated by a quadratic polynomial. The response surface was exhibited in a nonlinear concave shape, where only one minimum was expected. The values for the seven optimization parameters referring to this minimum were determined using the Downhill-Simplex algorithm [10].

3.4. Results of the optimization

The FE-model was updated using the optimized SCFs. The applied values for the optimization parameters are shown in table 5. The then computed radii and the comparison with the experimental ones are given in table 6.

Table 5: Optimized parameters A, B, C and D

Roll	SCF	OP	Solutions / optimized values
Setting roll	$F(u_1)$	A_1	0.365 mm
		B_1	1140 N
		C_1	12950 N
Bending roll	$F(u_2)$	A_2	0.495 mm
		B_2	957 N
		C_2	11135 N
Holding rolls	$F(u_3)$	D	9856 N

Table 6: Comparison of bending radii resulting from experiments, the initial FE-model and the optimized FE-model

Y-axis [°]	P-axis [°]	Experimental R_{exp} [mm]	Simulative R_{sim} [mm]	Optimized R_{opt} [mm]	Deviation R_{exp} and R_{sim} [%]	Deviation R_{exp} and R_{opt} [%]
35	34	75.54	78.51	77.60	-3.92	-2.73
	30	123.36	118.83	119.86	3.67	2.84
	27	206.39	193.24	204.73	6.37	0.98
	24.5	443.34	410.97	471.40	7.43	6.39

It can be seen that the precision of the optimized FE-model for characteristic line $Y=35^\circ$ is drastically improved for the surroundings of the radii 200mm. The accuracy for larger radii has also been improved slightly, however the results are still not within the required 5% deviation range.

3. Summary and outlook

The goal of the paper was to introduce an improved model of the three-roll-push-bending process. Special effort was to be put on the modeling of the machines deflection. This has been done by introducing spring and dashpot elements into the FE-model. Within this approach the spring's characteristic functions originally determined through static measurements were adjusted to the dynamic process conditions by means of optimization. The resulting FE-model showed good accuracy for a wide range of bending radii while using only little computation time. The presented FE-model provides the means to determine the required characteristic lines for a wide range of bending radii at acceptable computational cost and without the need for experiments or machine downtime at satisfying accuracy.

However, the simulated radii are not in satisfying accordance with the experimental ones even after the optimization. Further improvement is expected from a redefinition of the optimization parameters constrains, the used test plan. Some effort will be put in the definition of the objective function. At the moment the influence of all three rolls to the resulting bending radius is considered equal in so far, as all have the same influence on the objective function. But experiments show, that the influence of the setting roll is much more significant than that of the others. This should be addressed in the model and considered during optimization and might lead to a further improve in accuracy.

Moreover it will be interesting to use the optimized FE-model for the simulation of tubes with different geometries and different material properties. At first it has to be seen if the FE-model is providing the same accuracy for different semi finished products. If there is an influence of the material or the tubes geometry on the simulations accuracy, this might provide a starting point to research the effects of springback on the three-roll-push-bending process and the resulting bending radii.

References

- [1] Gantner, P.; Bauer, H.; Harrison, D. K.; De Silva, A. K. M.: Free-Bending – A new bending technique in the hydroforming process chain, *Journal of Materials Processing Technology*, 167 (2005), pp. 302-308
- [2] Merklein, M.; Hagenah, H.; Cojutti, M.: Investigation on Three-Roll Bending of Plain Tubular Components, *Key Engineering Materials*, 410-411 (2009), pp. 325-334
- [3] Hagenah, H.; Vipavc, D.; Vatter, P. H.; Cojutti, M.; Plettke, R.: Creation of the Data Base for the Process Design of the Three-Roll-Push Bending Process, *7th CIRP International Conference on Intelligent Computation in Manufacturing Engineering*, Capri 2010, accepted
- [4] Cojutti, M.; Vipavc, D.; Hagenah, H.; Merklein, M.: An Innovative Approach for the Process Design for Three-Roll Bending of Plain Tubular Components, *Proceedings of the International Congress on Efficient Rollforming*, Bilbao, Spain, 2009, pp. 133-139.
- [5] Plettke, R.; Vatter, P. H.; Vipavc, D.; Cojutti M.; Hagenah, H.: Investigation on the Process Parameters and Process Window of Three-Roll-Push-Bending, *Paper No: 1662-36th MATADOR Conference*, Manchester 2010, accepted
- [6] Sze, K. Y.; Liu, X. H.; Lo, S. H.: Popular benchmark problems for geometric nonlinear analysis of shells, *Finite Elements in Analysis and Design*, 40 (2004), pp. 1551-1569
- [7] Merklein, M., Charakterisierung von Blechwerkstoffen für den Leichtbau, Bamberg: Meisenbach Verlag, 2006
- [8] Hibbeler, R.C.: Engineering Mechanics, Statics and Dynamics, 10th Edition, Prentice Hall, 2003
- [9] Abaqus 6.8 Analysis User's Manuals; Volume VI: Elements; Chapter 18: Special-Purpose Elements
- [10] Nelder, J. A.; Mead, R. A.: A Simplex Method for Function Minimization, *Computer Journal*, 7 (1965), pp. 308-313